Available online at www.sciencedirect.com
ScienceDirect
Comput. Methods Appl. Mech. Engrg. 341 (2018) 939–955
Computer methods in applied mechanics and engineering
www.elsevier.com/locate/cma

A new strain smoothing method for triangular and tetrahedral finite elements

Chaemin Lee, Phill-Seung Lee*

Department of Mechanical Engineering, Korea Advanced Institute of Science and Technology, 291 Daehak-ro, Yuseong-gu, Daejeon 34141, Republic of Korea

Received 17 April 2018; received in revised form 6 July 2018; accepted 18 July 2018
Available online 23 July 2018

Highlights

- We propose a new strain smoothing method for triangular and tetrahedral finite elements.
- Linear strain fields are constructed within elements without using special smoothing domains.
- The proposed strain-smoothed elements pass patch, isotropic and zero energy mode tests.
- Its improved performance is demonstrated through various numerical examples.

Abstract

This paper presents a simple and effective strain smoothing method (the strain-smoothed element method) for 3-node triangular and 4-node tetrahedral solid finite elements. While piecewise constant strain fields are constructed through smoothing domains in previous strain smoothing methods, in the proposed method, linear strain fields are constructed within finite elements using constant strains of neighboring finite elements. When the new strain smoothing method is adopted, the triangular and tetrahedral solid finite elements pass all the basic tests; patch, isotropy and zero energy mode tests, and show improved predictive capability. The formulation of the proposed method is presented in detail. Through various numerical examples, we demonstrate the accuracy improvement achieved.

Keywords: Finite elements; Strain smoothing; Strain-smoothed element method; Solid elements; Triangular elements; Tetrahedral elements

1. Introduction

The finite element method (FEM) has been widely used for solving problems in various engineering fields over the past several decades [1,2]. There are various types of finite elements for analysis of solid mechanics problems, among which low-order finite elements such as 3-node triangular elements and 4-node tetrahedral elements are very attractive due to their simplicity and efficiency. However, in general, the predictive capability of low-order elements

* Corresponding author.
E-mail address: phillseung@kaist.edu (P.S. Lee).

https://doi.org/10.1016/j.cma.2018.07.022
0045-7825/

is not good enough to be used in engineering practice [3]. Further development of low-order finite elements with improved accuracy is still required while maintaining its advantages.

Recently, the smoothed finite element method (S-FEM) was developed and successfully applied to various mechanics problems [4–23]. The concept of S-FEM started from the strain smoothing technique proposed by Chen et al. for the Galerkin mesh-free method [24]. The strain smoothing technique was later applied to the finite element method. In S-FEM, the strain smoothing technique is applied to smooth the strain field of standard FEM. Piecewise constant strain fields are constructed in newly established smoothing domains.

In S-FEM, the smoothing domains can be constructed on the basis of a cell, node, edge, or face; thus, cell-based, node-based, edge-based, and face-based S-FEM methods were devised [4–23]. There are differences in characteristics and performance among the methods, and edge-based S-FEM is generally known to be most effective [13–19]. Compared to standard FEM, S-FEM achieves significantly improved accuracy, especially for 3-node triangular and 4-node tetrahedral solid finite elements. The important advantage of S-FEM is that no additional degrees of freedom (DOFs) are required, while for other methods, such as extended FEM and enriched FEM, additional DOFs are required to improve accuracy [25,26].

In this paper, we propose a new strain smoothing method (the strain-smoothed element method) that is useful for finite element analysis of problems in two-dimensional (2D) and three-dimensional (3D) solid mechanics. The standard 3-node triangular and 4-node tetrahedral finite elements have constant strain fields within elements, and the aforementioned S-FEM methods provide piecewise constant strain fields through smoothing domains.

The distinct feature of the strain-smoothed element (SSE) method is that special smoothing domains are not created, and that linear strain fields are constructed within elements. The linear strain field of an element is synthesized utilizing the constant strains of neighboring finite elements through simple strain smoothing. In this way, we obtain the full advantages of strain smoothing, and have a smoothed strain field integrated within the element. The strain-smoothed element method is simple and provides more accurate solutions in a variety of numerical examples than with the standard FEM, and with the face-based and edge-based S-FEM methods.

In the following sections, the formulation of the strain-smoothed element method is given for a 3-node triangular 2D solid element and for a 4-node tetrahedral 3D solid element. The performance of the proposed method is demonstrated through basic and convergence tests.

2. Strain smoothing for the 3-node triangular element

In this section, we briefly review the edge-based strain smoothing method [13–19], and present the formulation of the strain-smoothed element (SSE) method, for the 3-node triangular element for analysis of 2D solid mechanics problems.

2.1. Edge-based strain smoothing method

Here, we review the formulation of the edge-based strain smoothing method, which is applied to 3-node triangular finite elements. The geometry of the standard 3-node triangular 2D solid element is described by

$$\mathbf{x} = \sum_{i=1}^{3} h_i(r,\ s)\mathbf{x}_i \quad \text{with } \mathbf{x}_i = \begin{bmatrix} x_i & y_i \end{bmatrix}^T, \tag{1}$$

where $\mathbf{x}_i$ is the position vector of node i in the global Cartesian coordinate system, and $h_i(r, s)$ is the 2D interpolation function of the standard isoparametric procedure corresponding to node i given by

$$h_1 = 1 - r - s,\ h_2 = r,\ h_3 = s. \tag{2}$$

The displacement of the standard 3-node triangular 2D solid element is interpolated by

$$\mathbf{u} = \sum_{i=1}^{3} h_i(r,\ s)\mathbf{u}_i \quad \text{with } \mathbf{u}_i = \begin{bmatrix} u_i & v_i \end{bmatrix}^T, \tag{3}$$

where $\mathbf{u}_i$ is the displacement vector of node i in the global Cartesian coordinate system.

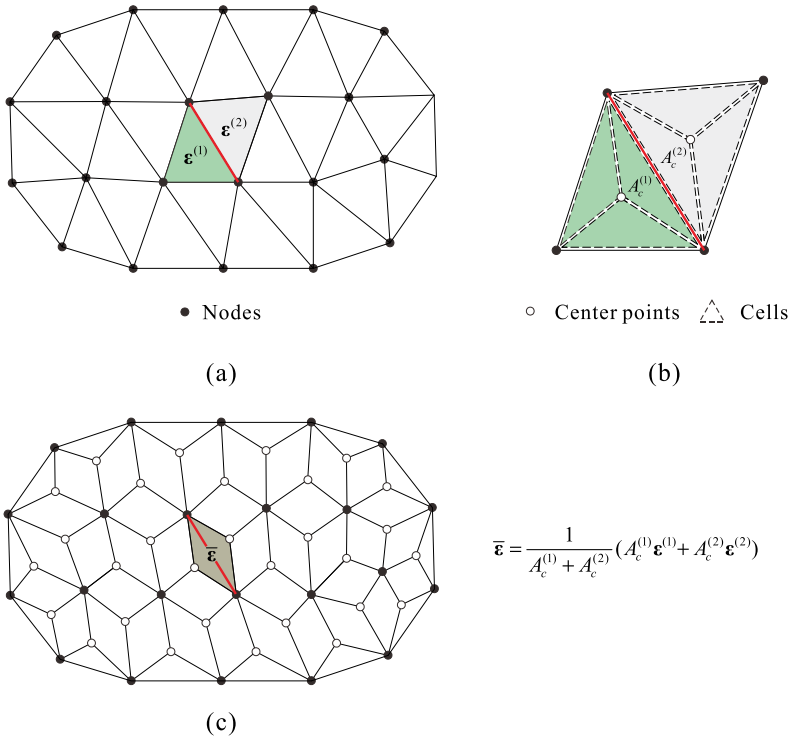

Fig. 1. Construction of edge-based smoothed strain fields: (a) Elements of the standard FEM. The red line corresponds to a target edge. (b) The elements are divided into three cells. (c) Smoothing domains and smoothed strains of the edge-based S-FEM. Piecewise constant strain fields are constructed for elements in (a) and for smoothing domains in (c). (For interpretation of the references to color in this figure legend, the reader is referred to the web version of this article.)

Employing the standard isoparametric finite element procedure, the strain field within a 3-node triangular element is obtained using

$$\boldsymbol{\varepsilon}^{(e)} = \mathbf{B}^{(e)}\mathbf{u}^{(e)} \quad \text{with } \mathbf{B}^{(e)} = \begin{bmatrix}\mathbf{B}_1 & \mathbf{B}_2 & \mathbf{B}_3\end{bmatrix}, \mathbf{u}^{(e)} = [\mathbf{u}_1 \quad \mathbf{u}_2 \quad \mathbf{u}_3]^T, \tag{4}$$

in which $\boldsymbol{\varepsilon}^{(e)} = [\varepsilon_{xx} \quad \varepsilon_{yy} \quad 2\varepsilon_{xy}]^T$, $\mathbf{B}^{(e)}$ is the strain–displacement matrix of an element, $\mathbf{u}^{(e)}$ is the nodal displacement vector of the element, and $\mathbf{B}_i$ is the strain–displacement matrix corresponding to node i.

Using the standard isoparametric procedure with Eq. (1) to (3), the matrix $\mathbf{B}_i$ in Eq. (4) can be represented by

$$\mathbf{B}_i = \frac{1}{2A^{(e)}}\begin{bmatrix} b_i & 0 \\ 0 & c_i \\ c_i & b_i \end{bmatrix} \quad \text{with } b_i = y_j - y_k, c_i = x_k - x_j; i, j, k = 1, 2, 3, \tag{5}$$

where $A^{(e)}$ is the area of the element, and b_i and c_i are obtained by the cyclic permutation of indexes i, j, k. The standard 3-node triangular finite element gives a constant strain field within the element.

In the edge-based strain smoothing method, smoothing domains are formed based on elements in standard FEM (shown in Fig. 1a). Let us consider two elements adjacent to the target edge painted in red in the figure. Each element is divided into three sub-triangles using its nodes and a center point ($r = s = 1/3$), and each sub-triangle is named "cell", see Fig. 1(b). In the red edge considered, the edge-based smoothing domain is defined as an assemblage of two neighboring cells belonging to different elements.

The smoothed strain for the edge-based smoothing domain is given by

$$\bar{\boldsymbol{\varepsilon}} = \frac{1}{A_c^{(1)} + A_c^{(2)}}(A_c^{(1)}\boldsymbol{\varepsilon}^{(1)} + A_c^{(2)}\boldsymbol{\varepsilon}^{(2)}), \tag{6}$$

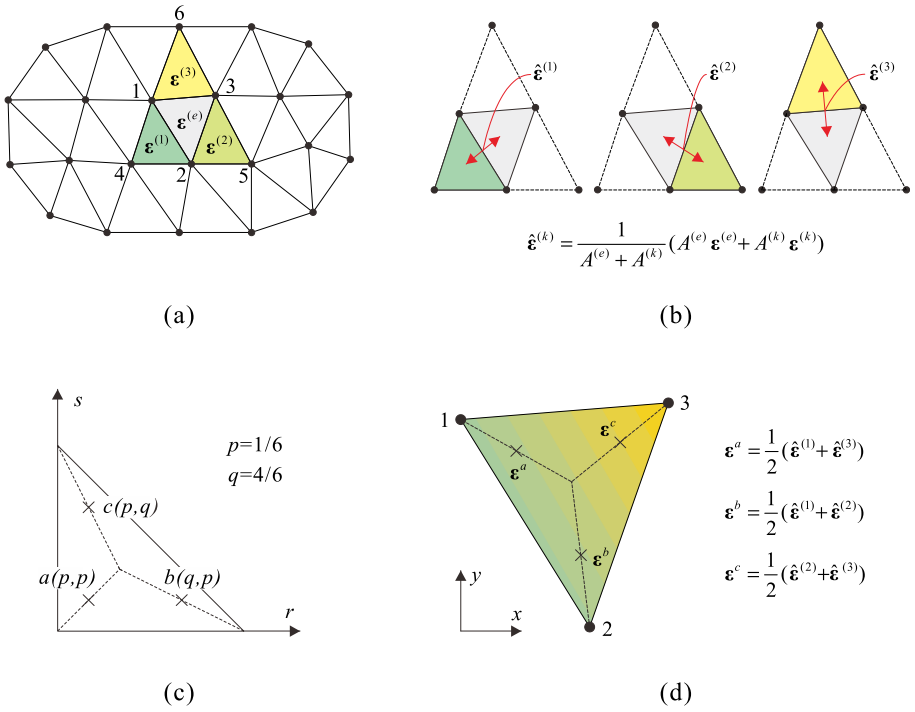

Fig. 2. Strain-smoothed element method for the 3-node triangular element: (a) Strains of a target element and its neighboring elements. Node numbers are used for explaining the formulation. (b) Strain smoothing between the target and each neighboring element. (c) Three Gauss integration points in the natural coordinate system (r, s). (d) Construction of the smoothed strain field through Gauss points.

where $A_c^{(1)}$ and $A_c^{(2)}$ are the areas of the first and second cells neighboring the target edge, and $\boldsymbol{\varepsilon}^{(1)}$ and $\boldsymbol{\varepsilon}^{(2)}$ are the strains of the neighboring finite elements. While Fig. 1(a) shows a typical domain discretization in the standard FEM, smoothing domains are shown in Fig. 1(c).

The edge-based strain smoothing method also has a constant strain field in the smoothing domain. It is known that the 3-node triangular elements subject to the edge-based strain smoothing method pass all the basic tests (patch, isotropy, and zero energy mode tests), and that the edge-based strain smoothing method shows the best performance among various S-FEM methods. Thus, the edge-based smoothing method has been extended for polyhedral 3D solid elements (see Ref. [18] for its formulation).

2.2. Strain-smoothed element method

With the proposed method, the strains of all neighboring elements are fully utilized in the strain smoothing process. For 3-node triangular elements, the strains of up to three surrounding elements can be used through element edges (see Fig. 2a) where $\boldsymbol{\varepsilon}^{(e)}$ is the strain of a target element and $\boldsymbol{\varepsilon}^{(k)}$ is the strain of the kth neighboring element.

Let us define smoothed strains between the target element and neighboring elements

$$\hat{\boldsymbol{\varepsilon}}^{(k)} = \frac{1}{A^{(e)} + A^{(k)}}(A^{(e)}\boldsymbol{\varepsilon}^{(e)} + A^{(k)}\boldsymbol{\varepsilon}^{(k)}) \quad \text{with } k = 1, 2, 3, \tag{7}$$

where $A^{(e)}$ and $A^{(k)}$ are the areas of the target element and the kth neighboring element, respectively, see Fig. 2(b). Note that if the kth edge of the target element corresponds to a boundary, there is no neighboring element for the edge and thus we use $\hat{\boldsymbol{\varepsilon}}^{(k)} = \boldsymbol{\varepsilon}^{(e)}$.

Smoothed strains in Eq. (7) can also be expressed in a matrix and vector form as

$$\hat{\boldsymbol{\varepsilon}}^{(k)} = \hat{\mathbf{B}}^{(k)}\hat{\mathbf{u}}^{(k)} \quad \text{with } \hat{\mathbf{B}}^{(k)} = \left[\hat{\mathbf{B}}_1 \quad \hat{\mathbf{B}}_2 \quad \hat{\mathbf{B}}_3 \quad \hat{\mathbf{B}}_{k+3}\right], \hat{\mathbf{u}}^{(k)} = [\mathbf{u}_1 \quad \mathbf{u}_2 \quad \mathbf{u}_3 \quad \mathbf{u}_{k+3}]^T. \tag{8}$$

where $\hat{\mathbf{B}}^{(k)}$ and $\hat{\mathbf{u}}^{(k)}$ are the strain–displacement matrix and the corresponding displacement vector of the element for the smoothed strains $\hat{\boldsymbol{\varepsilon}}^{(k)}$. The subscript i in $\hat{\mathbf{B}}_i$ and $\mathbf{u}_i$ denotes the neighboring node number as shown in Fig. 2(a).

In the 3-node triangular element, three point Gauss integration is used to calculate the stiffness matrix. We directly assign the smoothed strain values in Eq. (7) to the Gauss points (a, b, and c in Fig. 2c) of the target element using the following equations, as shown in Fig. 2(d)

$$\boldsymbol{\varepsilon}^a = \frac{1}{2}(\hat{\boldsymbol{\varepsilon}}^{(1)} + \hat{\boldsymbol{\varepsilon}}^{(3)}), \qquad \boldsymbol{\varepsilon}^b = \frac{1}{2}(\hat{\boldsymbol{\varepsilon}}^{(1)} + \hat{\boldsymbol{\varepsilon}}^{(2)}), \qquad \boldsymbol{\varepsilon}^c = \frac{1}{2}(\hat{\boldsymbol{\varepsilon}}^{(2)} + \hat{\boldsymbol{\varepsilon}}^{(3)}). \tag{9}$$

Therefore, in the computation of the stiffness matrix and stress, the strains assigned in Eq. (9) are used directly at the Gauss integration points. The strain field within the element can be explicitly expressed in a form of assumed strain

$$\bar{\boldsymbol{\varepsilon}}^{(e)} = \left[1 - \frac{1}{q-p}(r+s-2p)\right]\boldsymbol{\varepsilon}^a + \frac{r-p}{q-p}\boldsymbol{\varepsilon}^b + \frac{s-p}{q-p}\boldsymbol{\varepsilon}^c, \tag{10}$$

where $p = 1/6$ and $q = 4/6$ are the constants indicating the positions of the Gauss points. Note that the use of this equation is not necessary in actual computations.

When the element has three neighboring elements with common element edges, the strain–displacement relation for the strain field can be expressed in a vector and matrix form as

$$\bar{\boldsymbol{\varepsilon}}^{(e)} = \bar{\mathbf{B}}^{(e)}\bar{\mathbf{u}}^{(e)}, \tag{11}$$

with

$$\bar{\mathbf{B}}^{(e)} = \left[\bar{\mathbf{B}}_1 \quad \bar{\mathbf{B}}_2 \quad \bar{\mathbf{B}}_3 \quad \bar{\mathbf{B}}_4 \quad \bar{\mathbf{B}}_5 \quad \bar{\mathbf{B}}_6\right], \tag{12}$$

$$\bar{\mathbf{u}}^{(e)} = \left[\mathbf{u}_1 \quad \mathbf{u}_2 \quad \mathbf{u}_3 \quad \mathbf{u}_4 \quad \mathbf{u}_5 \quad \mathbf{u}_6\right]^T, \tag{13}$$

where $\bar{\mathbf{B}}^{(e)}$ is the strain–displacement matrix of the strain-smoothed element, and $\bar{\mathbf{u}}^{(e)}$ is the corresponding displacement vector of the element. Note that the components of the strain–displacement matrix and the displacement vector vary depending on the configurations of neighboring elements.

As in other strain smoothing methods, exterior (boundary) elements have relatively fewer neighboring elements than interior elements and thus the strain smoothing effect in the exterior region could be less than that in the interior region.

3. Strain-smoothed 4-node tetrahedral element

The geometry of the standard 4-node tetrahedral 3D solid element is described by

$$\mathbf{x} = \sum_{i=1}^{4} h_i(r,\ s,\ t)\mathbf{x}_i \quad \text{with } \mathbf{x}_i = \left[x_i \quad y_i \quad z_i\right]^T, \tag{14}$$

where $\mathbf{x}_i$ is the position vector of node i in the global Cartesian coordinate system, and $h_i(r, s, t)$ is the 3D interpolation function of the standard isoparametric procedure corresponding to node i given by

$$h_1 = 1 - r - s - t,\ h_2 = r,\ h_3 = s,\ h_4 = t. \tag{15}$$

The displacement of the standard 4-node tetrahedral 3D solid element is given by

$$\mathbf{u} = \sum_{i=1}^{4} h_i(r,\ s,\ t)\mathbf{u}_i \quad \text{with } \mathbf{u}_i = \left[u_i \quad v_i \quad w_i\right]^T, \tag{16}$$

where $\mathbf{u}_i$ is the displacement vector of node i in the global Cartesian coordinate system.

The strain–displacement relation of the standard tetrahedral element is

$$\boldsymbol{\varepsilon}^{(e)} = \mathbf{B}^{(e)}\mathbf{u}^{(e)}, \tag{17}$$

with

$$\mathbf{B}^{(e)} = \left[\mathbf{B}_1 \quad \mathbf{B}_2 \quad \mathbf{B}_3 \quad \mathbf{B}_4\right], \mathbf{u}^{(e)} = [\mathbf{u}_1 \quad \mathbf{u}_2 \quad \mathbf{u}_3 \quad \mathbf{u}_4]^T, \tag{18}$$

where $\boldsymbol{\varepsilon}^{(e)} = [\varepsilon_{xx} \quad \varepsilon_{yy} \quad \varepsilon_{zz} \quad 2\varepsilon_{xy} \quad 2\varepsilon_{yz} \quad 2\varepsilon_{zx}]^T$, $\mathbf{B}^{(e)}$ is the strain–displacement matrix of an element, and $\mathbf{u}^{(e)}$ is the displacement vector of the element.

In Eq. (18), $\mathbf{B}_i$ is the strain–displacement matrix corresponding to node i calculated by

$$\mathbf{B}_i = \frac{1}{6V^{(e)}} \begin{bmatrix} b_i & 0 & 0 \\ 0 & c_i & 0 \\ 0 & 0 & d_i \\ c_i & b_i & 0 \\ 0 & d_i & c_i \\ d_i & 0 & b_i \end{bmatrix} \quad \text{with } i, j, k, l = 1, 2, 3, 4, \tag{19}$$

$$b_i = (-1)^i \det \begin{vmatrix} 1 & y_j & z_j \\ 1 & y_k & z_k \\ 1 & y_l & z_l \end{vmatrix}, \; c_i = (-1)^i \det \begin{vmatrix} x_j & 1 & z_j \\ x_k & 1 & z_k \\ x_l & 1 & z_l \end{vmatrix}, \; d_i = (-1)^i \det \begin{vmatrix} x_j & y_j & 1 \\ x_k & y_k & 1 \\ x_l & y_l & 1 \end{vmatrix}, \tag{20}$$

where b_i, c_i, and d_i are obtained by the cyclic permutation of indexes i,j,k,l.

In a tetrahedral element, configurations of neighboring elements through six element edges can differ. Smoothed strains between the target element and neighboring elements through the edges are calculated using the following equations

$$\hat{\boldsymbol{\varepsilon}}^{(k)} = \frac{1}{V^{(e)} + \sum_{i=1}^{n_k} V_i^{(k)}} \left(V^{(e)} \boldsymbol{\varepsilon}^{(e)} + \sum_{i=1}^{n_k} V_i^{(k)} \boldsymbol{\varepsilon}_i^{(k)} \right) \quad \text{with } k = 1, 2, 3, 4, 5, 6, \tag{21}$$

where n_k is the number of elements neighboring the kth edge of the target element, $\boldsymbol{\varepsilon}^{(e)}$ and $\boldsymbol{\varepsilon}_i^{(k)}$ are the strains of the target element and the ith element neighboring the kth edge of the target element, respectively. Here, $V^{(e)}$ and $V_i^{(k)}$ are the volumes of the target element and the ith element neighboring the kth edge, respectively, see Fig. 3(a). Note that if the kth edge of the target element is located alone along a boundary without neighboring elements, $n_k = 0$ and thus $\hat{\boldsymbol{\varepsilon}}^{(k)} = \boldsymbol{\varepsilon}^{(e)}$.

The stiffness matrix of the tetrahedral element is calculated using the four point Gauss integration, see the positions of the Gauss points a, b, c, and d in Fig. 3(b). The strains at the Gauss points are directly assigned using the following equations, as shown in Fig. 3(c)

$$\boldsymbol{\varepsilon}^a = \frac{1}{5}(\hat{\boldsymbol{\varepsilon}}^{(1)} + \hat{\boldsymbol{\varepsilon}}^{(2)} + \hat{\boldsymbol{\varepsilon}}^{(3)} + \hat{\boldsymbol{\varepsilon}} + \boldsymbol{\varepsilon}^{(e)}), \; \boldsymbol{\varepsilon}^b = \frac{1}{5}(\hat{\boldsymbol{\varepsilon}}^{(1)} + \hat{\boldsymbol{\varepsilon}}^{(4)} + \hat{\boldsymbol{\varepsilon}}^{(6)} + \hat{\boldsymbol{\varepsilon}} + \boldsymbol{\varepsilon}^{(e)}),$$

$$\boldsymbol{\varepsilon}^c = \frac{1}{5}(\hat{\boldsymbol{\varepsilon}}^{(2)} + \hat{\boldsymbol{\varepsilon}}^{(4)} + \hat{\boldsymbol{\varepsilon}}^{(5)} + \hat{\boldsymbol{\varepsilon}} + \boldsymbol{\varepsilon}^{(e)}), \; \boldsymbol{\varepsilon}^d = \frac{1}{5}(\hat{\boldsymbol{\varepsilon}}^{(3)} + \hat{\boldsymbol{\varepsilon}}^{(5)} + \hat{\boldsymbol{\varepsilon}}^{(6)} + \hat{\boldsymbol{\varepsilon}} + \boldsymbol{\varepsilon}^{(e)}) \quad \text{with } \hat{\boldsymbol{\varepsilon}} = \frac{1}{6} \sum_{k=1}^{6} \hat{\boldsymbol{\varepsilon}}^{(k)}. \tag{22}$$

The strain field can be represented by

$$\bar{\boldsymbol{\varepsilon}}^{(e)} = \left[1 - \frac{1}{q-p}(r + s + t - 3p) \right] \boldsymbol{\varepsilon}^a + \frac{r-p}{q-p} \boldsymbol{\varepsilon}^b + \frac{s-p}{q-p} \boldsymbol{\varepsilon}^c + \frac{t-p}{q-p} \boldsymbol{\varepsilon}^d, \tag{23}$$

with $p = (5 - \sqrt{5})/20$ and $q = (5 + 3\sqrt{5})/20$. Note that this assumed strain field is not used in actual computations.

Strain smoothing methods do not require additional DOFs, but some additional processes are necessary to perform strain smoothing. Several studies have validated the efficiency of the strain smoothing methods by evaluating their computational cost and accuracy. It has been reported that the edge-based strain smoothing method is the most efficient strain smoothing method so far [13,18]. The strain-smoothed element method proposed in this study shows computational cost similar to that of the edge-based strain smoothing method.

4. Basic numerical tests

For the proposed triangular and tetrahedral elements, we perform three basic numerical tests: the isotropy, patch and zero energy mode tests [1–3].

The isotropy test is to check whether the finite elements give the same results regardless of the node numbering sequences used. The proposed triangular and tetrahedral elements pass the isotropy test [3].

In the patch tests, the minimum number of degrees of freedom is constrained to prevent rigid body motions, and proper loadings are applied to produce a constant stress field. To satisfy the patch tests, a constant stress value should

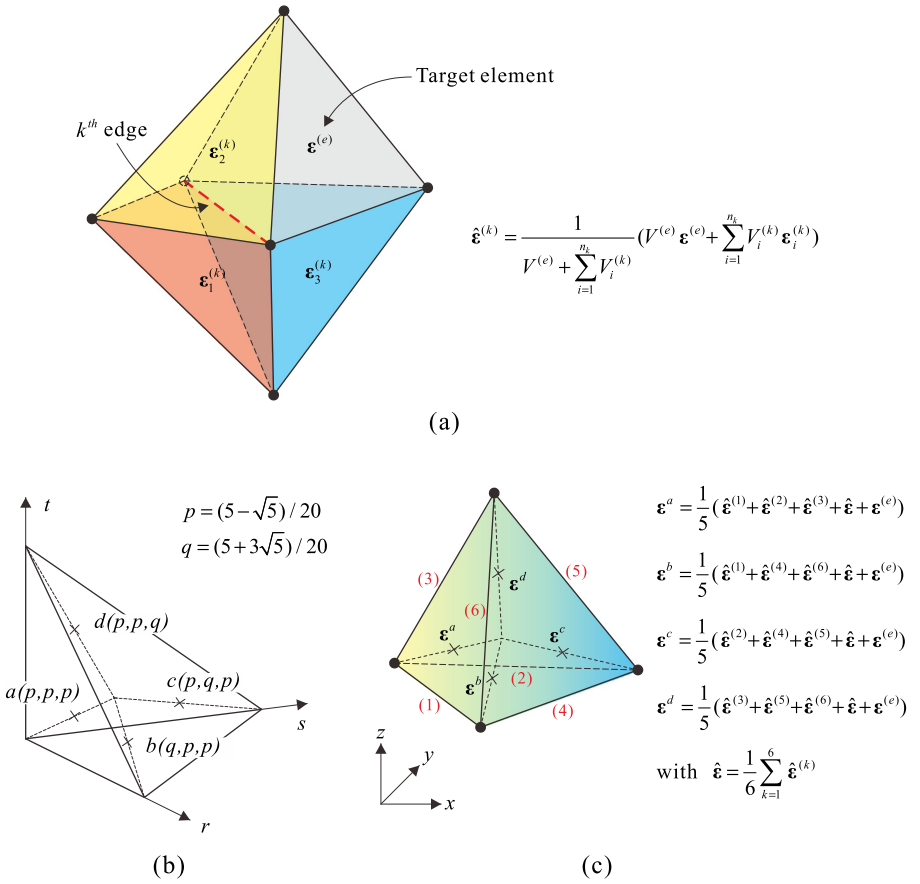

Fig. 3. Strain-smoothed element method for the 4-node tetrahedral element: (a) Strain smoothing between the target and neighboring elements for the kth edge of the target element marked with the red dotted line. There are three neighboring elements through the edge ($n_k = 3$). (b) Four Gauss integration points in the natural coordinate system (r, s, t). (c) Construction of the smoothed strain field through Gauss points. Edge numbers are colored in red.

be obtained at every point on elements. Normal and shear patch tests are performed using the meshes shown in Fig. 4. Stress values calculated (using 16 significant decimal digits of precision) are extracted from all Gauss integration points and compared with the analytical solutions. In the proposed triangular and tetrahedral elements, the maximum relative error in the normal and shear patch tests are on the order of 10^{-14} to 10^{-15}. Therefore, the proposed elements pass the patch tests with sufficient accuracy.

In the zero energy mode test, we count the number of zero eigenvalues of the stiffness matrix of unsupported smoothed elements. The 2D and 3D solid elements should have three and six zero eigenvalues, respectively, corresponding to the physical rigid body modes. The proposed elements pass the zero energy mode test.

5. Numerical examples

In this section, we present the performance of the strain-smoothed elements using three 2D numerical examples (a block problem, Cook's skew beam problem, and an infinite plate with a central hole problem), and two 3D numerical examples (a cubic cantilever problem and Lame problem).

The performance of the proposed 3-node triangular element is compared with those of the standard linear triangular finite element and edge-based smoothed finite element. The performance of the proposed 4-node tetrahedral element is compared with those of the standard linear tetrahedral finite element, edge-based, and face-based smoothed finite elements [13–21]. The edge-based and face-based smoothed elements are denoted by ES-FEM and FS-FEM, respectively.

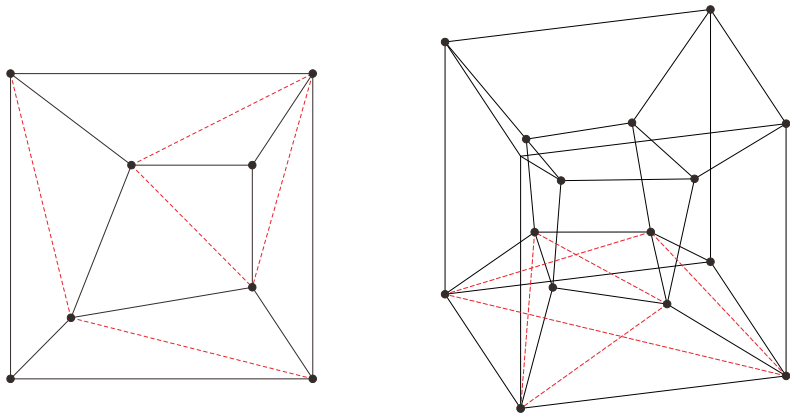

Fig. 4. Finite element meshes used for the patch tests: (a) 2D patch test. Each quadrilateral element is divided into two triangular elements. (b) 3D patch test. Each hexahedral element is divided into six tetrahedral elements. Only the splits in the hexahedral element located at the bottom are depicted.

In some examples, we compare the performance of the proposed triangular and tetrahedral elements with those of the standard quadratic 6-node triangular and 10-node tetrahedral elements, respectively. On the convergence curves, the element size is defined as $h = 1/N$ for linear elements and $h = 1/2N$ for quadratic elements. This allows comparison of linear and quadratic elements with the same DOFs.

We compare the displacements and stresses at a specific location. We also use energy norm. The relative error in the energy norm is given by

$$E_e^2 = \frac{\left| \left\| \mathbf{u}_{ref} \right\|_e^2 - \left\| \mathbf{u}_h \right\|_e^2 \right|}{\left\| \mathbf{u}_{ref} \right\|_e^2} \quad \text{with } \|\mathbf{u}\|_e^2 = \int_\Omega \boldsymbol{\varepsilon}^T \boldsymbol{\sigma} d\Omega, \tag{24}$$

where the subscripts "ref" and "h" denote the reference and finite element solutions, respectively.

For the relative error in the energy norm, the optimal convergence behavior for the linear elements is estimated to be

$$E_e^2 \cong ch^2, \tag{25}$$

in which c is a constant and h denotes the element size [1].

5.1. Block problem

Here, we solve the 2D block problem shown in Fig. 5(a). The block is subjected to a distributed compression force of total magnitude $P = 1$ at the right half of the top edge, and the bottom edge of the block is clamped. Plane stress conditions are assumed with $E = 3 \times 10^7$ and $\nu = 0.3$, and density is given as $\rho = 1 \times 10^7$. We use structured meshes of $N \times N$ elements with $N = 2$, 4, 8 and 16 (shown in Fig. 5b), and unstructured meshes with the total number of elements $N_e = 6$, 32, 128, 500 (Fig. 5c). The unstructured meshes are acquired through the commercial software ANSYS. The equivalent values of N in the unstructured meshes are calculated by $N = \sqrt{N_e/2}$.

Table 1 gives the predicted vertical displacement at point A for the structured mesh. Fig. 6 gives the convergence curves obtained using the energy norm for both structured and unstructured meshes. The reference solutions are obtained using a 32×32 structured mesh of 9-node quadrilateral solid elements. The use of the proposed element gives much more accurate solutions than when using the standard and edge-based smoothed elements.

In addition, free vibration analysis is performed to compare the performance of the finite elements considered. The generalized eigenvalue problem is defined as

$$\mathbf{K}\boldsymbol{\varphi}_i = \lambda_i \mathbf{M}\boldsymbol{\varphi}_i \quad \text{with } i = 1, 2, \ldots, n, \tag{26}$$

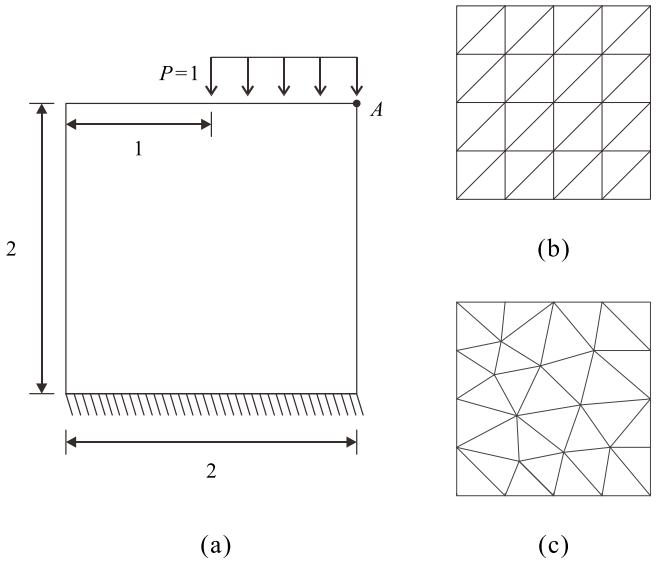

Fig. 5. 2D block problem: (a) Problem description ($E = 3 \times 10^7$ and $\nu = 0.3$). (b) Structured mesh used with $N = 4$. (c) Unstructured mesh used with $N_e = 32$.

Table 1
Vertical displacement ($\times 10^{-8}$) at point A in the block problem. The values in parentheses indicate relative errors obtained by $\left|u_{ref} - u_h\right| / u_{ref} \times 100$.

N	Standard FEM	ES-FEM	SSE (proposed)
2	−5.7442 (26.71)	−7.3025 (6.82)	−8.1969 (4.59)
4	−6.9824 (10.91)	−7.7441 (1.19)	−7.8770 (0.51)
8	−7.5945 (3.10)	−7.8176 (0.25)	−7.8431 (0.07)
	Reference solution: −7.8372		

Table 2
Eigenvalues corresponding to the 1st–5th modes for the 2D block problem when the structured mesh with $N = 4$ is adopted.

Mode	Reference	Standard FEM	ES-FEM	SSE (proposed)
1	0.3249	0.3828	0.3465	0.3327
2	1.8713	1.9249	1.8934	1.8759
3	2.3552	2.8456	2.4728	2.3634
4	5.9470	7.8848	6.4520	5.7638
5	6.9164	8.5072	7.5547	7.0044

where $\mathbf{K}$ and $\mathbf{M}$ are the global stiffness and consistent mass matrices, respectively, λ_i and $\boldsymbol{\varphi}_i$ are the eigenvalue and eigenvector corresponding to the ith mode, respectively, and n denotes the number of DOFs in the finite element model. Table 2 presents the obtained eigenvalues corresponding to the 1st–5th modes for the structured mesh with $N = 4$. The proposed element performs very well.

5.2. Cook's skew beam problem

We next consider Cook's skew beam problem [27], as shown in Fig. 7. The structure is subjected to distributed shearing force of total magnitude $P = 1$ at the right edge, and the left edge of the structure is clamped. The plane stress conditions with $E = 3 \times 10^7$ and $\nu = 0.3$ are considered. The solutions are obtained with $N \times N$ element meshes ($N = 2$, 4, 8, and 16).

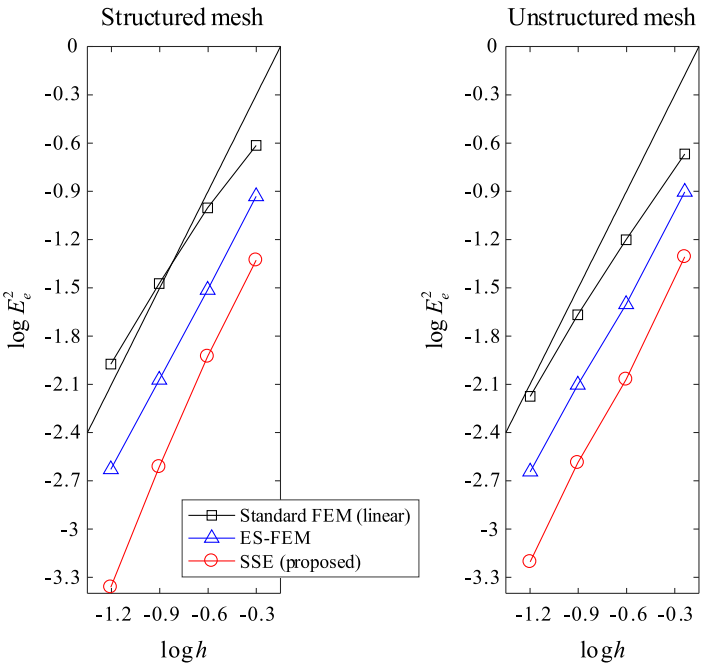

Fig. 6. Convergence curves for the 2D block problem. The bold line represents the optimal convergence rate.

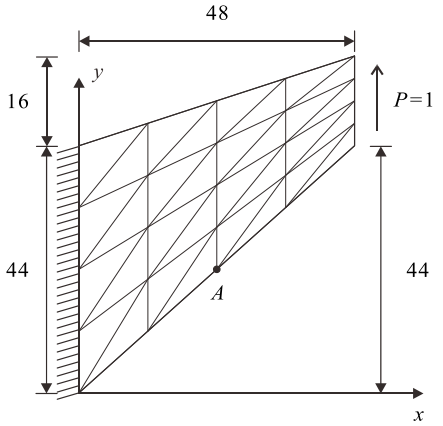

Fig. 7. Cook's skew beam problem (4 × 4 mesh, $E = 3 \times 10^7$ and $\nu = 0.3$).

Fig. 8 shows the distribution of the calculated strain component $2\varepsilon_{xy}$. The proposed triangular element shows the strain field most similar to the reference distribution. Table 3 gives the von-Mises stress at point A, shown in Fig. 7. The stress values are obtained by averaging stresses in the domains (elements in the proposed method) to which the point belongs. Fig. 9 shows the convergence curves obtained using the energy norm. A 32 × 32 element mesh of 9-node 2D solid elements is used for the reference solutions. The proposed element shows much better convergence behavior than do the standard linear element and edge-based smoothed element. Interestingly, the convergence performance of the proposed (linear) element is comparable to that of the standard quadratic element.

5.3. Infinite plate with a central hole problem

The last 2D example is the problem of an infinite plate with a central hole [4]. The plate is subjected to a far field traction $p = 1$ in the x-direction as shown in Fig. 10(a). The plane strain conditions are considered with $E = 3 \times 10^7$

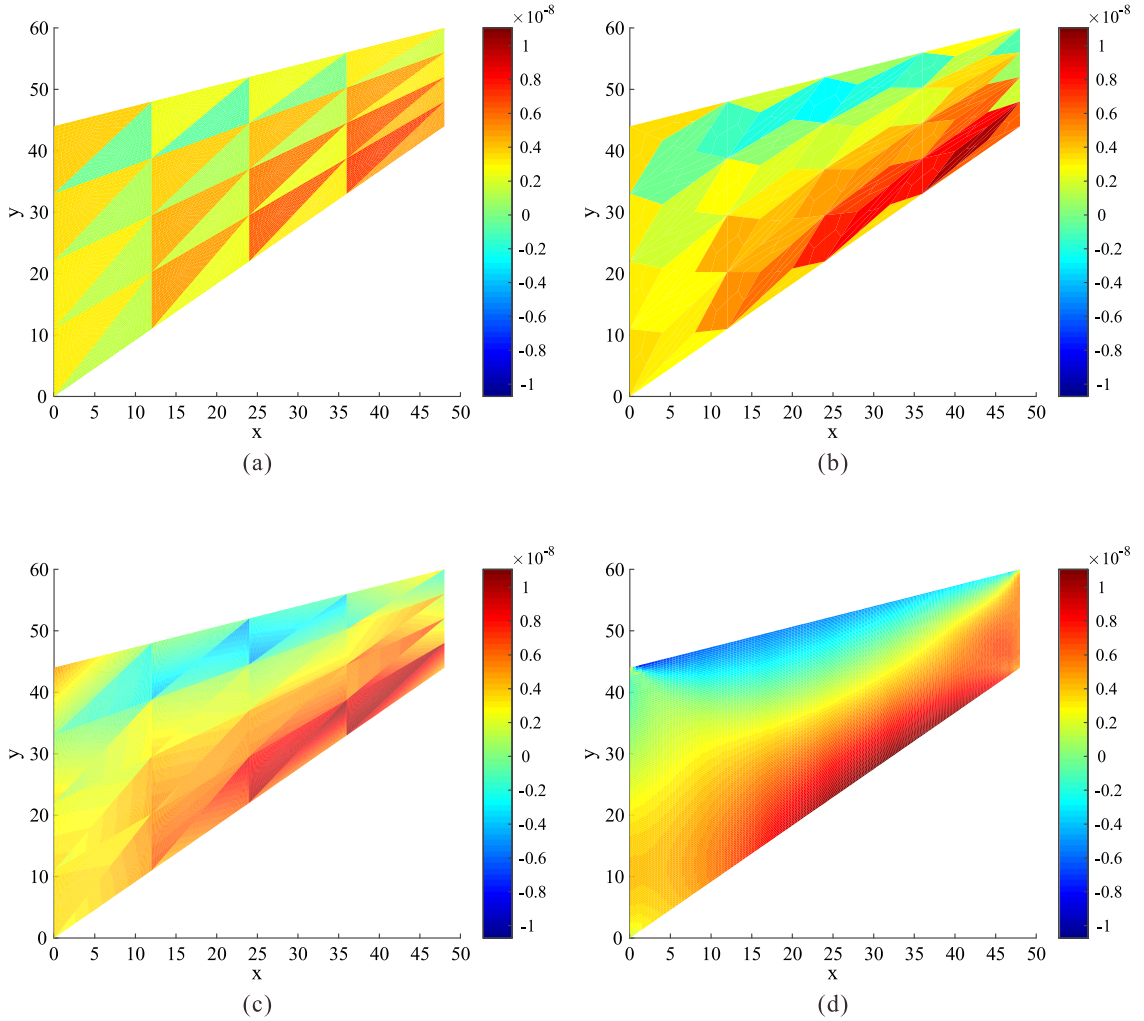

Fig. 8. Strain distributions ($2\varepsilon_{xy}$) calculated for Cook's skew beam problem: (a) Standard 3-node triangular element ($N = 4$), (b) Edge-based smoothed element ($N = 4$), (c) Strain-smoothed triangular element ($N = 4$), (d) Standard 9-node quadrilateral element ($N = 32$).

Table 3
von-Mises stress at point A in Cook's skew beam problem. The values in parentheses indicate relative errors obtained by $\left|\sigma_{ref} - \sigma_h\right| / \sigma_{ref} \times 100$.

N	Standard FEM	ES-FEM	SSE (proposed)
2	0.0740 (68.77)	0.1009 (57.43)	0.1209 (48.99)
4	0.1123 (52.63)	0.1889 (20.33)	0.2105 (11.19)
8	0.1685 (28.90)	0.2228 (6.03)	0.2290 (3.40)
	Reference solution: 0.2371		

and $\nu = 0.3$. Due to its symmetry, only one-quarter of the plate is modeled. Symmetric boundary conditions are imposed: $u_x = 0$ along AC and $u_y = 0$ along BD, and the traction boundary conditions are imposed along CE and DE based on the following analytical solutions [28]:

Table 4
Horizontal displacement ($\times 10^{-8}$) at point B in the infinite plate with central hole problem. The values in parentheses indicate relative errors obtained by $\left|u_{ref} - u_h\right| / u_{ref} \times 100$.

N	Standard FEM	ES-FEM	SSE (proposed)
2	6.0622 (33.38)	7.5364 (17.18)	8.3902 (7.80)
4	7.3026 (19.75)	8.2955 (8.84)	8.7312 (4.05)
8	8.2250 (9.62)	8.7763 (3.56)	8.9807 (1.31)
	Analytical solution: 9.1000		

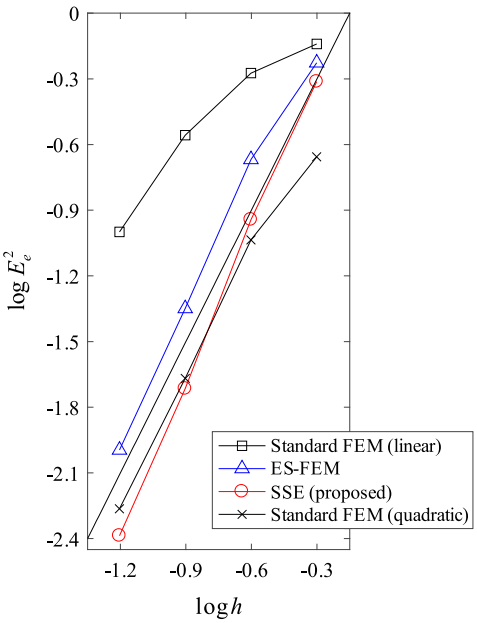

Fig. 9. Convergence curves for Cook's skew beam problem: The bold line represents the optimal convergence rate for the linear elements. The element size is $h = 1/N$ for the linear elements and $h = 1/2N$ for the quadratic element.

$$\sigma_{11}(r,\theta) = p - \frac{pa^2}{r^2}\left[\frac{3}{2}\cos 2\theta + \cos 4\theta\right] + \frac{3pa^4}{2r^4}\cos 4\theta, \tag{27}$$

$$\sigma_{22}(r,\theta) = -\frac{pa^2}{r^2}\left[\frac{1}{2}\cos 2\theta - \cos 4\theta\right] - \frac{3pa^4}{2r^4}\cos 4\theta, \tag{28}$$

$$\sigma_{12}(r,\theta) = -\frac{pa^2}{r^2}\left[\frac{1}{2}\sin 2\theta + \sin 4\theta\right] + \frac{3pa^4}{2r^4}\sin 4\theta, \tag{29}$$

where r is the distance from the origin and θ is the angle from the positive x-axis to the counterclockwise direction. The geometry is divided into two parts and meshed for each part using $N \times N$ elements with $N = 2, 4, 8$ and 16, see Fig. 10(b).

Table 4 and Fig. 11 show the horizontal displacement at point B and the convergence curves obtained using the energy norm, respectively. To obtain the reference solution, a mesh of 9-node 2D solid elements is used with $N = 32$. Compared with standard and edge-based smoothed elements, the proposed element shows significantly improved accuracy.

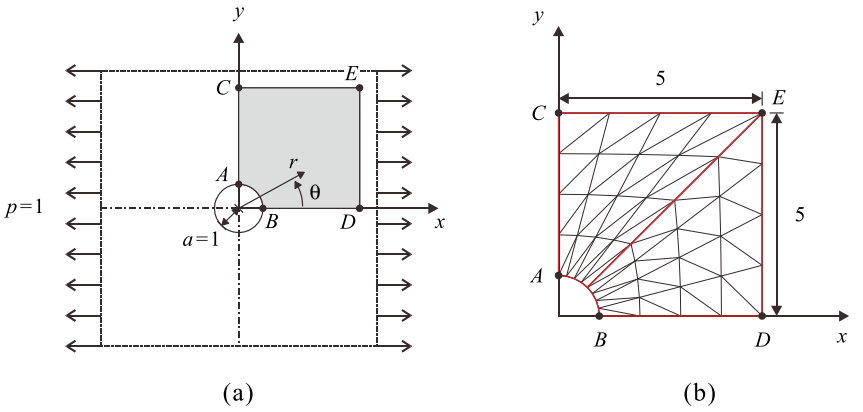

Fig. 10. Infinite plate with central hole problem: (a) Problem description ($E = 3 \times 10^7$ and $\nu = 0.3$). (b) Mesh used with $N = 4$ for the shaded domain in (a).

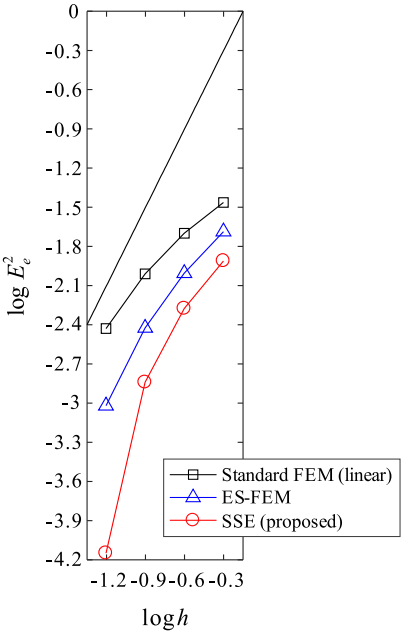

Fig. 11. Convergence curves for the infinite plate with central hole problem. The bold line represents the optimal convergence rate.

5.4. Cubic cantilever problem

Here, we solve the 3D cubic cantilever problem [29] shown in Fig. 12(a). The cubic cantilever is subjected to a uniform pressure $p = 1$ on its upper surface, and the outer surface on the xz-plane is clamped. The material properties are $E = 1$, $\nu = 0.25$, and $\rho = 1$. We use two types of mesh: structured mesh of $N \times N \times N$ elements with $N = 2, 4$, and 8 (see Fig. 12b), and unstructured mesh of $N_e = 63$, 352, and 2973 (see Fig. 12c). The equivalent values of N in the unstructured meshes are obtained using $N = \sqrt[3]{N_e/6}$.

Table 5 gives the calculated eigenvalues corresponding to the 1st–5th modes for the structured mesh with $N = 4$. Fig. 13 shows the convergence curves obtained using the energy norm for the structured and unstructured meshes. A structured $16 \times 16 \times 16$ mesh of 27-node hexahedral solid finite elements is used for the reference solutions. The use of the proposed tetrahedral element gives better solutions than when using the standard linear elements and when

Table 5
Eigenvalues corresponding to the 1st–5th modes for the 3D cubic cantilever problem when the structured mesh with $N = 4$ is adopted.

Mode	Reference	Standard FEM	FS-FEM	ES-FEM	SSE (proposed)
1	0.4484	0.5137	0.4946	0.4633	0.4509
2	0.4484	0.5471	0.5211	0.4791	0.4668
3	0.8563	1.1884	1.0718	0.9147	0.8791
4	2.5216	2.6204	2.5970	2.5527	2.5328
5	3.1823	3.7323	3.5445	3.2582	3.1645

Table 6
von-Mises stress at point G in Lame problem. The values in parentheses indicate relative errors obtained by $\left|\sigma_{ref} - \sigma_h\right| / \sigma_{ref} \times 100$.

N	Standard FEM	FS-FEM	ES-FEM	SSE (proposed)
2	106.2858 (38.00)	125.3865 (26.86)	150.2877 (12.33)	166.7563 (2.73)
4	132.7286 (22.58)	143.6493 (16.20)	157.3288 (8.22)	166.3370 (2.97)
8	149.4181 (12.84)	155.2355 (9.45)	162.2212 (5.37)	166.6823 (2.77)
16	159.4205 (7.00)	162.5707 (5.17)	167.5228 (2.28)	169.5621 (1.09)
	Analytical solution: 171.4286			

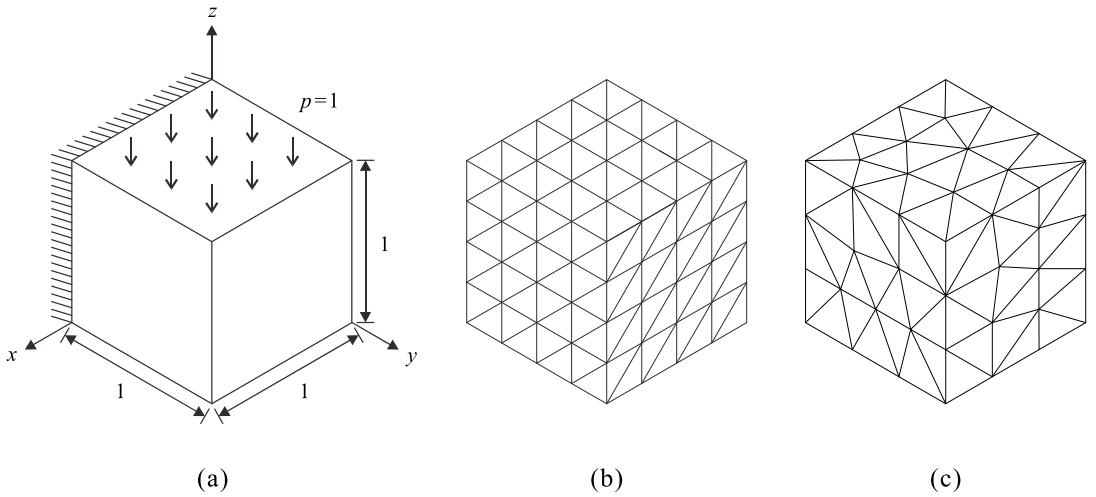

Fig. 12. Cubic cantilever problem: (a) Problem description ($E = 1$ and $\nu = 0.25$). (b) Structured mesh with $N = 4$. (c) Unstructured mesh with $N_e = 352$.

using either face-based smoothed or edge-based smoothed elements. It is also observed that the performance of the proposed (linear) element is comparable to that of the standard quadratic element.

5.5. Lame problem

We last consider the 3D Lame problem [28] shown in Fig. 14(a). A hollow sphere is subjected to internal pressure $p = 100$, and the given material properties are $E = 1 \times 10^3$ and $\nu = 0.3$. Utilizing the symmetry condition, only one-eighth of the structure is considered. It is divided into three parts, each of which is meshed using $N \times N \times N$ elements with $N = 2$, 4, and 8 (see Fig. 14b). The symmetric boundary conditions imposed are $u_x = 0$ along $ACFE$, $u_y = 0$ along $BDFE$, and $u_z = 0$ along $CABD$.

Table 6 shows the von-Mises stress at point G, obtained by averaging stresses in the domains (elements in the proposed method) to which the point belongs. Fig. 15 presents the convergence curves obtained using the energy norm. A mesh of 27-node hexahedral solid finite elements with $N = 16$ is used for the reference solution. It is again observed that the proposed element shows significantly improved convergence behavior compared to the standard linear, face-based smoothed, and edge-based smoothed elements.

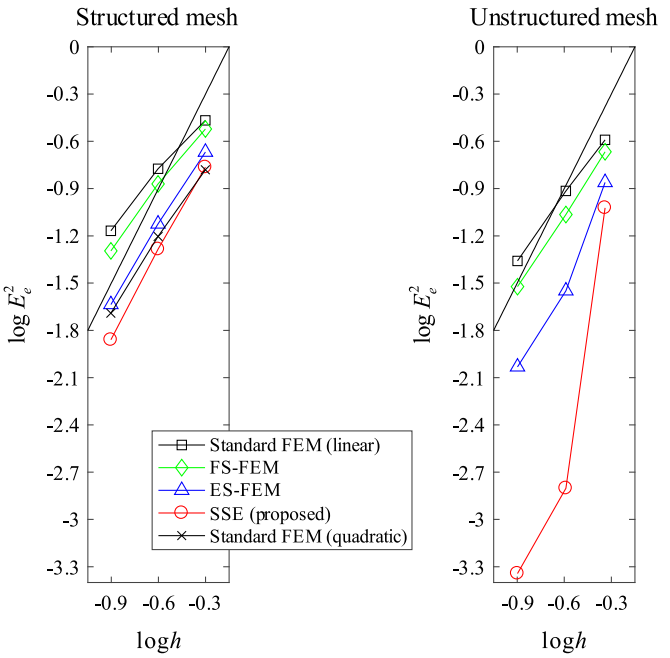

Fig. 13. Convergence curves for the cubic cantilever problem: The bold line represents the optimal convergence rate for the linear elements. The element size is $h = 1/N$ for the linear elements and $h = 1/2N$ for the quadratic element.

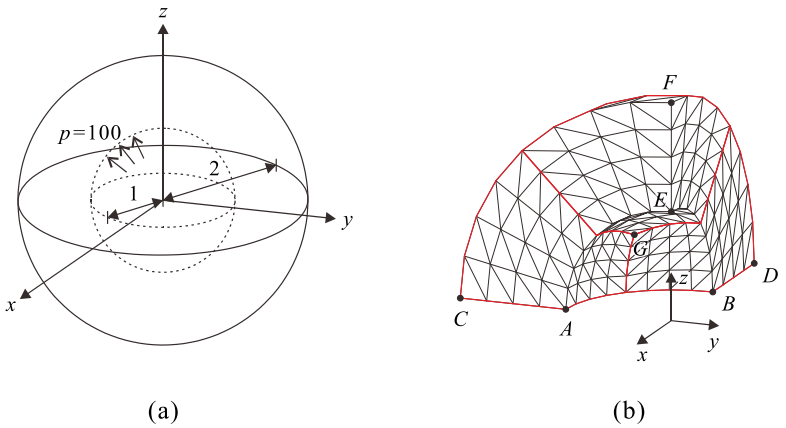

Fig. 14. Lame problem: (a) Problem description ($E = 1 \times 10^3$ and $\nu = 0.3$). (b) Mesh used with $N = 4$.

6. Concluding remarks

In this paper, we proposed a new strain smoothing method (the strain-smoothed element method), for 3-node triangular and 4-node tetrahedral finite elements. To construct a smoothed strain field of a target element, the strains of neighboring elements were utilized. The smoothed strain values were directly assigned to the Gauss integration points of the element. Consequently, strain-smoothed triangular and tetrahedral elements were developed. Unlike with previous S-FEM methods, special smoothing domains are not created in the strain-smoothed element (SSE) method. That is, the domain discretization is the same as with the standard finite element method. The strain-smoothed triangular and tetrahedral elements give linear strain fields within elements.

The proposed elements passed patch, isotropy, and zero energy mode tests, and showed improved convergence behavior, when compared to the standard and edge-based smoothed elements in 2D, and the standard, face-based and

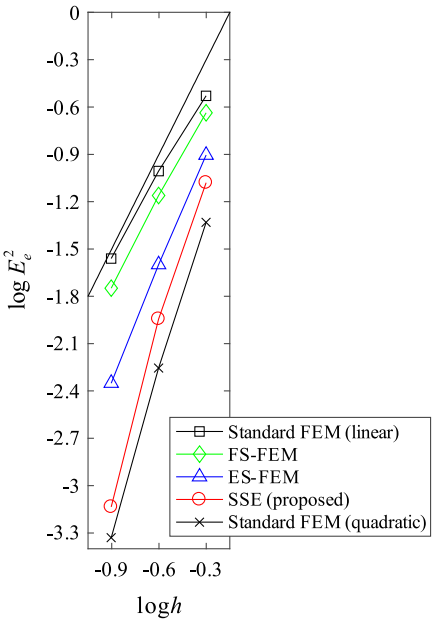

Fig. 15. Convergence curves for Lame problem: The bold line represents the optimal convergence rate for the linear elements. The element size is $h = 1/N$ for the linear elements and $h = 1/2N$ for the quadratic element.

edge-based smoothed elements in 3D solid mechanics problems. The SSE method could easily be applied for other solid elements and also for beam, plate and shell elements [3,30–36]. It could also be used effectively to solve material and geometric nonlinear problems [11,21].

Acknowledgments

This work was supported by the National Research Foundation of Korea (NRF) grant funded by the Korea government (MSIT) (No. NRF-2018R1A2B3005328). This work was also supported by "Human Resources Program in Energy Technology" of the Korea Institute of Energy Technology Evaluation and Planning (KETEP), granted financial resource from the Ministry of Trade, Industry & Energy, Republic of Korea (No. 20184030202000).

References

[1] K.J. Bathe, in: K.J. Bathe, Watertown (Eds.), Finite Element Procedures, Vol. 2014, second ed., Higher Education Press, China, 2016.
[2] T.J.R. Hughes, The Finite Element Method: Linear Static and Dynamic Finite Element Analysis, Dover Publications, Mineola, NY, 2000.
[3] P.S. Lee, K.J. Bathe, Development of MITC isotropic triangular shell finite elements, Comput. Struct. 82 (2004) 945–962.
[4] G.R. Liu, K.Y. Dai, T.T. Nguyen, A smoothed finite element method for mechanics problems, Comput. Mech. 39 (2007) 859–877.
[5] N. Nguyen-Thanh, T. Rabczuk, H. Nguyen-Xuan, S.P.A. Bordas, A smoothed finite element method for shell analysis, Comput. Methods Appl. Mech. Engrg. 198 (2008) 165–177.
[6] S.P.A. Bordas, T. Rabczuk, N.X. Hung, V.P. Nguyen, S. Natarajan, T. Bog, D.M. Quan, N.V. Hiep, Strain smoothing in FEM and XFEM, Comput. Struct. 88 (2010) 1419–1443.
[7] P. Phung-Van, T. Nguyen-Thoi, H. Luong-Van, Q. Lieu-Xuan, Geometrically nonlinear analysis of functionally graded plates using a cell-based smoothed three-node plate element (CS-MIN3) based on the C0-HSDT, Comput. Methods Appl. Mech. Engrg. 270 (2014) 15–36.
[8] P. Phung-Van, T. Nguyen-Thoi, H. Dang-Trung, N. Nguyen-Minh, A cell-based smoothed discrete shear gap method (CS-FEM-DSG3) using layerwise theory based on the C0-HSDT for analyses of composite plates, Compos. Struct. 111 (2014) 553–565.
[9] A. Hamrani, S.H. Habib, I. Belaidi, CS-IGA: A new cell-based smoothed isogeometric analysis for 2D computational mechanics problems, Comput. Methods Appl. Mech. Engrg. 315 (2017) 671–690.
[10] G.R. Liu, T. Nguyen-Thoi, H. Nguyen-Xuan, K.Y. Lam, A node-based smoothed finite element method (NS-FEM) for upper bound solutions to solid mechanics problems, Comput. Struct. 87 (2009) 14–26.
[11] T. Nguyen-Thoi, H.C. Vu-Do, T. Rabczuk, H. Nguyen-Xuan, A node-based smoothed finite element method (NS-FEM) for upper bound solution to visco-elastoplastic analyses of solids using triangular and tetrahedral meshes, Comput. Methods Appl. Mech. Engrg. 199 (2010) 3005–3027.

[12] G. Wang, X.Y. Cui, H. Feng, G.Y. Li, A stable node-based smoothed finite element method for acoustic problems, Comput. Methods Appl. Mech. Engrg. 297 (2015) 348–370.
[13] G.R. Liu, T. Nguyen-Thoi, K.Y. Lam, An edge-based smoothed finite element method (ES-FEM) for static, free and forced vibration analyses of solids, J. Sound Vib. 320 (2009) 1100–1130.
[14] Z.C. He, G.R. Liu, Z.H. Zhong, S.C. Wu, G.Y. Zhang, A.G. Cheng, An edge-based smoothed finite element method (ES-FEM) for analyzing three-dimensional acoustic problems, Comput. Methods Appl. Mech. Engrg. 199 (2009) 20–33.
[15] L. Chen, T. Rabczuk, S.P.A. Bordas, G.R. Liu, K.Y. Zeng, P. Kerfriden, Extended finite element method with edge-based strain smoothing (ESm-XFEM) for linear elastic crack growth, Comput. Methods Appl. Mech. Engrg. 209–212 (2012) 250–265.
[16] H. Nguyen-Xuan, G.R. Liu, S. Bordas, S. Natarajan, T. Rabczuk, An adaptive singular ES-FEM for mechanics problems with singular field of arbitrary order, Comput. Methods Appl. Mech. Engrg. 253 (2013) 252–273.
[17] C.M. Shin, B.C. Lee, Development of a strain-smoothed three-node triangular flat shell element with drilling degrees of freedom, Finite Elem. Anal. Des. 86 (2014) 71–80.
[18] C. Lee, H. Kim, S. Im, Polyhedral elements by means of node/edge-based smoothed finite element method, Internat. J. Numer. Methods Engrg. 110 (2016) 1069–1100.
[19] C. Lee, H. Kim, J. Kim, S. Im, Polyhedral elements using an edge-based smoothed finite element method for nonlinear elastic deformations of compressible and nearly incompressible materials, Comput. Mech. 60 (2017) 659–682.
[20] T. Nguyen-Thoi, G.R. Liu, K.Y. Lam, G.Y. Zhang, A face-based smoothed finite element method (FS-FEM) for 3D linear and geometrically non-linear solid mechanics problems using 4-node tetrahedral elements, Internat. J. Numer. Methods Engrg. 78 (2009) 324–353.
[21] T. Nguyen-Thoi, G.R. Liu, H.C. Vu-Do, H. Nguyen-Xuan, A face-based smoothed finite element method (FS-FEM) for visco-elastoplastic analyses of 3D solids using tetrahedral mesh, Comput. Methods Appl. Mech. Engrg. 198 (2009) 3479–3498.
[22] D. Sohn, J. Han, Y.S. Cho, S. Im, A finite element scheme with the aid of a new carving technique combined with smoothed integration, Comput. Methods Appl. Mech. Engrg. 254 (2013) 42–60.
[23] S. Jin, D. Sohn, S. Im, Node-to-node scheme for three-dimensional contact mechanics using polyhedral type variable-node elements, Comput. Methods Appl. Mech. Engrg. 304 (2016) 217–242.
[24] J.S. Chen, S. Yoon, C.T. Wu, A stabilized conforming nodal integration for Galerkin mesh-free methods, Internat. J. Numer. Methods Engrg. 53 (2001) 2587–2615.
[25] I. Babuška, J.M. Melenk, The partition of unity method, Internat. J. Numer. Methods Engrg. 40 (1997) 727–758.
[26] T.P. Fries, T. Belytschko, The extended/generalized finite element method: An overview of the method and its applications, Internat. J. Numer. Methods Engrg. 84 (2010) 253–304.
[27] R.D. Cook, Concepts and Applications of Finite Element Analysis, John Wiley & Sons, New York, 2007.
[28] S.P. Timoshenko, J.N. Goodier, Theory of Elasticity, third ed., McGraw-Hill, New York, 1970.
[29] Y. Yang, G. Sun, H. Zheng, A four-node tetrahedral element with continuous nodal stress, Comput. Struct. 191 (2017) 180–192.
[30] S. Kim, P.S. Lee, A new enriched 4-node 2D solid finite element free from the linear dependence problem, Comput. Struct. 202 (2018) 25–43.
[31] M.L. Bucalem, K.J. Bathe, Higher-order MITC general shell elements, Internat. J. Numer. Methods Engrg. 36 (1993) 3729–3754.
[32] P.S. Lee, K.J. Bathe, On the asymptotic behavior of shell structures and the evaluation in finite element solutions, Comput. Struct. 80 (2002) 235–255.
[33] K.J. Bathe, D. Chapelle, P.S. Lee, A shell problem "highly sensitive" to thickness changes, Internat. J. Numer. Methods Engrg. 57 (2003) 1039–1052.
[34] Y. Lee, P.S. Lee, K.J. Bathe, The MITC3+ shell element and its performance, Comput. Struct. 138 (2014) 12–23.
[35] H.M. Jeon, Y. Lee, P.S. Lee, K.J. Bathe, The MITC3+ shell element in geometric nonlinear analysis, Comput. Struct. 146 (2015) 91–104.
[36] Y. Lee, H.M. Jeon, P.S. Lee, K.J. Bathe, The modal behavior of the MITC3+ triangular shell element, Comput. Struc. 153 (2015) 148–164.